12. sEPSPs were detected separately at each recording site with the use of a sliding template algorithm (*30*) following digital filtering (2 kHz) and displayed together with the voltage response recorded simultaneously at the other recording sites on a fast time base. sEPSPs were accepted as being generated near a recording site if they were fastest rising at that site and had a rise time of less than 3 ms. Experiments with aEPSPs demonstrated that the local amplitude of dendritic EPSPs increased as they were generated more distally. Consequently, at dendritic sites, our procedures detected events generated by EPSCs that would be undetectable if generated at perisomatic sites. To correct for this finding, the threshold amplitude for sEPSP detection was increased for dendritic recording sites on the basis of the experimentally observed increase in local aEPSP amplitude (a procedure that would increase the chance of observing synaptic scaling). The efficacy of event detection was verified by detection of all unitary EPSPs during paired recordings. EPSP rise time represents 10 to 90%, and half-width the duration at half amplitude.
13. The kinetics of dendritic sEPSPs were unrelated to amplitude at each recording site [see (*21*)].
14. aEPSPs were generated with exponentially rising (0.2 ms) and decaying (2 ms) waveforms of 200-pA amplitude. Kinetics were based on published estimates (*31*) and reproduced the time course of dendritically generated EPSPs (sEPSPs: rise time 1.11 ± 0.05 ms, half-width 5.97 ± 0.30 ms; aEPSPs: rise time 1.29 ± 0.08 ms, half-width 6.75 ± 0.26 ms).
15. Neurons were morphological identified following visualization of neurobiotin (0.5 to 2% in pipette solution) staining with standard procedures. We were unable to directly visualize the site of putative contacts made by layer 2/3 pyramidal neuron axons. Single uEPSPs were evoked every 3 s; during paired-pulse experiments uEPSPs were evoked every 5 s, and during action potential trains every 10 s.
16. S. Redman, B. Walmsley, *J. Physiol. (London)* **343**, 117 (1983).
17. uEPSPs with fast somatic kinetics were of smaller amplitude and slower at dendritic recording sites, whereas slow somatic uEPSPs were larger and had faster kinetics at dendritic recording sites.
18. These findings cannot be accounted for by changes in local driving force because during repetitive activation at 40 Hz, each distal dendritic uEPSPs would be expected to have decayed close to baseline before generation of subsequent EPSPs (see Figs. 1B, 2A, and 4A).
19. M. Hausser, N. Spruston, G. J. Stuart, *Science* **290**, 739 (2000).
20. G. M. Shepherd, *et al.*, *Proc. Natl. Acad. Sci. U.S.A.* **82**, 2192 (1985).
21. Supplementary Web material is available on *Science* Online at www.sciencemag.org/cgi/content/full/295/5561/1907/DC1.
22. The different time window for integration of dendritic and somatic EPSPs results from contrasting local EPSP time courses (dendrite: 6.8 ± 0.3 ms half-width; soma: 18.0 ± 0.9 ms). The longer duration of somatic aEPSPs is a product of neuronal geometry and recruitment of perisomatic noninactivating sodium channels (*32, 33*).
23. Local EPSP amplitude will be greatest in the apical tuft of layer 5 pyramidal neurons, where initiation of dendritic spikes will be most efficacious (*34*), reducing the number of coincident EPSPs required for dendritic spike initiation.
24. D. B. Jaffe, N. T. Carnevale, *J. Neurophysiol.* **82**, 3268 (1999).
25. S. J. Redman, *J. Physiol. (London)* **234**, 637 (1973).
26. O. Bernander, R. J. Douglas, K. A. C. Martin, C. Koch, *Proc. Natl. Acad. Sci. U.S.A.* **88**, 11569 (1991).
27. R. Llinas, U. Ribary, D. Contreras, C. Pedroarena, *Philos. Trans. R. Soc. London B Biol. Sci.* **353**, 1841 (1998).
28. C. D. Gilbert, *Neuron* **9**, 1 (1992).
29. S. R. Williams, G. J. Stuart, *J. Physiol. (London)* **521**, 467 1999).
30. J. D. Clements, J. M. Bekkers, *Biophys. J.* **73**, 220 1997.
31. M. Hausser, A. Roth, *J. Neurosci.* **17**, 7606 1997.
32. C. Koch, M. Rapp, I. Segev, *Cereb. Cortex* **6**, 93 1996.
33. G. Stuart, B. Sakmann, *Neuron* **15**, 1065 1995.
34. See P. A. Rhodes, R. R. Llinas, *J. Physiol. (London)* **536**, 167 2001.
35. We thank A. T. Gulledge and B. M. Kampa for helpful discussions. Supported by the Wellcome Trust.

9 November 2001; accepted 15 January 2002

Parallel Single-Cell Monitoring of Receptor-Triggered Membrane Translocation of a Calcium-Sensing Protein Module

Mary N. Teruel and Tobias Meyer*

Time courses of translocation of fluorescently conjugated proteins to the plasma membrane were simultaneously measured in thousands of individual rat basophilic leukemia cells. We found that the C2 domain—a calcium-sensing, lipid-binding protein module that is an essential regulator of protein kinase C and numerous other proteins—targeted proteins to the plasma membrane transiently if calcium was released from internal stores, and persistently in response to entry of extracellular calcium across the plasma membrane. The C2 domain translocation time courses of stimulated cells clustered into only two primary modes. Hence, the reversible recruitment of families of signaling proteins from one cellular compartment to another is a rapid bifurcation mechanism for inducing discrete states of cellular signaling networks.

Studies of the dynamic behavior of signaling systems require the measurement of signaling time courses in individual living cells, because critical cell-to-cell differences are lost in averaged bulk cell measurements (*1, 2*). One of the most prominent dynamic cell signaling events is the receptor-triggered translocation of signaling proteins with SH2 (Src homology 2), PH (pleckstrin homology), C1, C2, and related domains from the cytosol to the plasma membrane (*3, 4*). In particular, calcium-sensing C2 domains that exist in kinases, lipases, and many other enzymes and regulatory proteins (*5, 6*) are intriguing examples of translocation domains because they target signaling proteins to lipid membranes in response to ubiquitously triggered Ca^{2+} signals (*7, 8*).

We developed an imaging technology based on large-area evanescent wave excitation to simultaneously measure the plasma membrane translocation of the C2 domain from protein kinase Cγ (PKCγ) fused to yellow fluorescent protein (YFP) [YFP–C2 domain] (*9*) in thousands of living rat basophilic leukemia (RBL) cells. In this evanescent wave single-cell array technology (E-SCAT; Fig. 1, A and B) [Web table 1 and Web fig. 1 (*10*)], cells are grown on a thin glass plate that serves as a uniform guide for laser light with an evanescent field that

Department of Molecular Pharmacology, Stanford University Medical School, 269 Campus Drive, Stanford, CA 94305, USA.

*To whom correspondence should be addressed. E-mail: tobiasmeyer@stanford.edu

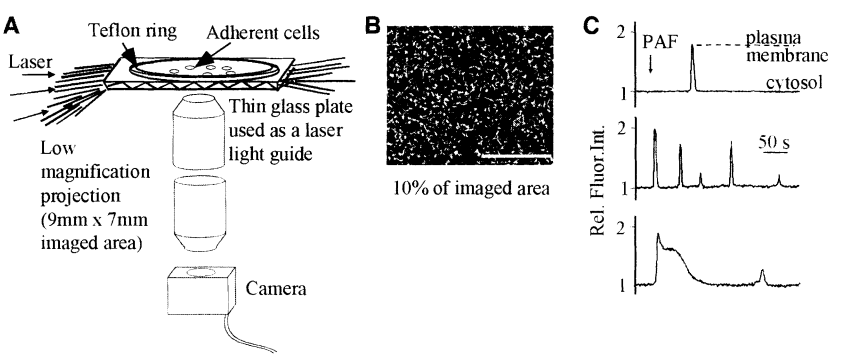

Fig. 1. Simultaneous measurement of plasma membrane translocation events in thousands of individual cells. (**A**) Schematic view of the E-SCAT system. In this method, an evanescent field is generated above a large surface area by coupling a laser into the angled edge (15°) of a glass plate 200 μm thick (*10, 29*). A high numerical aperture projection system was built to image a 7 mm by 9 mm region at the glass-water interface onto a CCD camera (*30*). Up to ~100,000 cells can be plated in this region. (**B**) A 10% subregion of an E-SCAT image used for translocation time course analysis [full image shown in Web fig. 3 (*10*)]. Each bright spot reflects a transfected RBL cell whose surface plasma membrane is excited by evanescent wave excitation. Scale bar, 1 mm. (**C**) Representative time courses of relative fluorescence intensity reflecting three single-cell translocation events in RBL cells transfected with YFP–C2 domain after addition of a submaximal concentration of PAF (final concentration 1 nM).

penetrates less than 100 nm above the glass surface (*11, 12*). Because fluorescent molecules at the plasma membrane near the glass surface are selectively excited over those in the cytosol, the translocation of signaling proteins to the plasma membrane in response to the activation of receptors on the cell surface can be measured as increases in local fluorescence intensity over time. Figure 1C shows translocation time courses measured, after the addition of 1 nM platelet activating factor (PAF), in RBL cells transfected with YFP–C2 domain (*9*). Control experiments with cells expressing YFP alone showed no increases in the fluorescent signals.

We developed software tools (*13*) to analyze the fluorescence intensity changes over time in each cell transfected with the YFP–C2 domain construct and measured translocation time courses at different concentrations of PAF. Pattern analysis showed that the translocation in individual cells can be described by one of two responses: a transient response in which the C2 domains translocated to the plasma membrane and rapidly dissociated again after 5.5 ± 2 s (full width at half-maximum ± SD; N = 6102 transients), and a persistent response in which the domain translocated and remained at the plasma membrane for more than 30 s (Fig. 2A). Multiple cell recordings were overlaid on a surface plot for each range of PAF concentrations. As depicted, the z axis is proportional to the number of cells with a particular normalized translocation signal (y axis) at a specified time (x axis). The fluorescent signal from 10 s before to 30 s after the peak translocation was normalized with the peak translocation set to 1. The time courses at PAF concentrations below 1 nM consisted primarily of transient responses, and those at concentrations above 10 nM consisted primarily of persistent responses, whereas intermediate agonist concentrations triggered a mixture of discrete transient and persistent responses (Fig. 2A). Only a small number of measured responses were outside these two principal response patterns.

About half of the C2 domains that have been characterized biochemically bind to lipid membranes in the presence of two or three Ca^{2+} ions (*7, 14, 15*), and membrane translocation events have been reported to be preceded by an increase in the concentration of intracellular free Ca^{2+} ($[Ca^{2+}]_i$) (*16*). A mutation of Asp^{187} to Asn^{187} (*17*) that reduces Ca^{2+}-mediated C2 domain membrane binding in vitro (*18*) also reduced the PAF-induced C2 domain translocation; this result is consistent with a direct role of Ca^{2+} in mediating C2 domain translocation. The increase in fluorescence after application of 100 nM PAF was 29.3 ± 2.4% (mean ± SE; N = 615 cells) for the mutant C2 domain, compared to 240.7 ± 3.1% for the wild type (N = 1900 cells).

Cytosolic Ca^{2+} signals can be triggered by Ca^{2+} release from intracellular stores or by Ca^{2+} influx across the plasma membrane (*19*), so we tested whether the two sources of Ca^{2+} might generate the observed translocation patterns. Cells exposed to 300 pM PAF triggered transient translocation events that were unaffected by the removal of extracellular Ca^{2+} (N = 810 of 815 cells; Fig. 2B, left), which suggests that the transient response pattern largely stems from release of Ca^{2+} from intracellular stores. In cells exposed to 10 nM PAF, the persistent translocation of C2 domains observed in the presence of extracellular Ca^{2+} (N = 2579 of 2611 cells; Fig. 2B, center) was abolished when extracellular Ca^{2+} was removed (N = 1835 of 1835 cells; Fig. 2B, right). The C2 domains returned to the cytosol in less than 1 min.

Addition of thapsigargin, which blocks calcium pumps in intracellular stores (*20*), led to persistent C2 domain translocation in the presence of extracellular Ca^{2+} (N = 700 of 700 cells; Fig. 2C, left) and only a transient localization in the absence of extracellular Ca^{2+} (N = 1321 of 1365 cells; Fig. 2C, center). This result is consistent with a requirement of Ca^{2+} influx for persistent C2 domain plasma membrane localization. Addition of extracellular Ca^{2+} to cells pretreated with thapsigargin in the absence of extracellular Ca^{2+} induced a persistent C2 domain plasma membrane localization (N = 1365 of 1365 cells; Fig. 2C, right). In control measurements, addition of 100 nM PAF to cells pretreated with thapsigargin in the absence of extracellular Ca^{2+} did not elicit a translocation response (*21*), which suggests that PAF does not activate alternative Ca^{2+}-independent translocation pathways. Thus, although calcium release triggers the initial membrane translocation, calcium influx appears to be the principal driving force for retaining C2 domains at the plasma membrane.

Many signaling processes exhibit first-order kinetics with effective activities proportional to both the duration and the amplitude of a signal (*22, 23*). In contrast, signaling processes that desensitize respond selectively to rapid signal increases while rejecting slower increases (*24*). These findings suggest that the integral of a signal over time and the rate of increase of a signal are two important

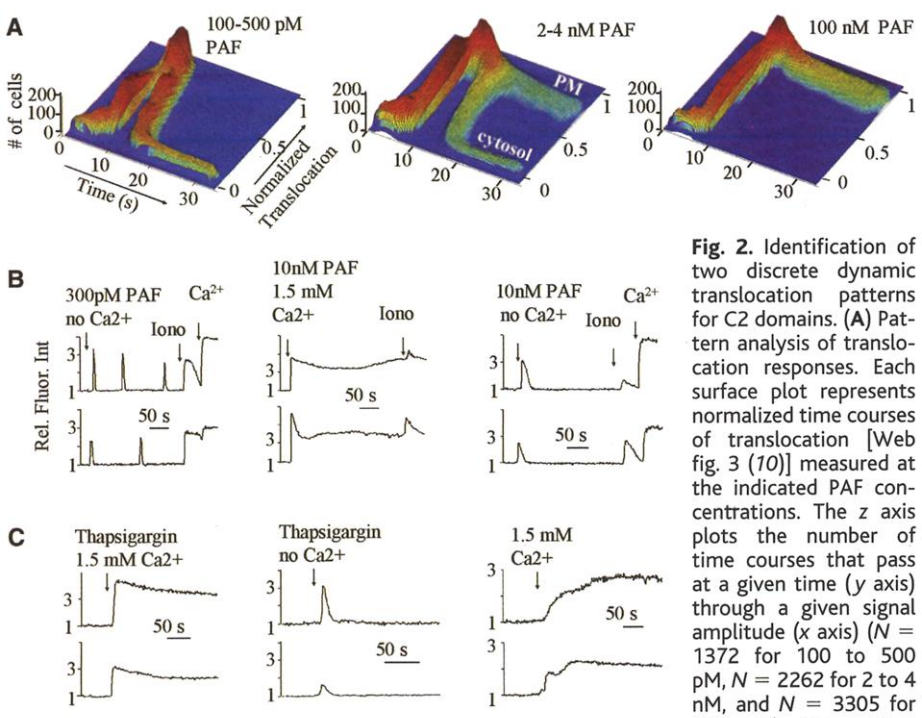

Fig. 2. Identification of two discrete dynamic translocation patterns for C2 domains. (**A**) Pattern analysis of translocation responses. Each surface plot represents normalized time courses of translocation [Web fig. 3 (*10*)] measured at the indicated PAF concentrations. The z axis plots the number of time courses that pass at a given time (y axis) through a given signal amplitude (x axis) (N = 1372 for 100 to 500 pM, N = 2262 for 2 to 4 nM, and N = 3305 for 100 nM). The surface plots were generated by 100 × 100 binning and 12 × 12 low-pass filtering. (**B**) C2 domain translocation events triggered by PAF in the absence of extracellular Ca^{2+} (extracellular addition of 2.5 mM Mg-EGTA). The responses at 300 pM PAF in the absence of extracellular Ca^{2+} (left panel) had spikes indistinguishable from those seen in experiments at 100 to 500 pM PAF in the presence of extracellular Ca^{2+}. However, the C2 domain translocation responses at a PAF concentration of 10 nM were persistent in the presence of extracellular Ca^{2+} (center panel) and transient without extracellular Ca^{2+} (right panel), suggesting that the persistent localization of C2 domains requires Ca^{2+} influx. Ionomycin and calcium were added at the end to calibrate the translocation response. (**C**) Transient versus persistent plasma membrane localization of C2 domains in the presence of thapsigargin, a blocker of intracellular Ca^{2+} pumps. Left panel: Addition of 5 μM thapsigargin triggers persistent plasma membrane localization. Center panel: In the absence of extracellular Ca^{2+}, the thapsigargin-induced translocation has only a small amplitude and is transient. Right panel: Addition of Ca^{2+} to cells pretreated with thapsigargin in the absence of extracellular Ca^{2+} triggers persistent C2 domain translocation.

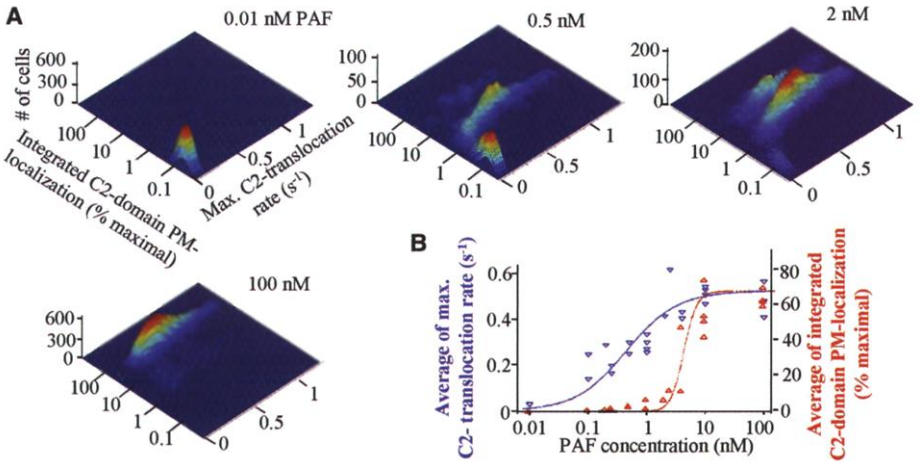

Fig. 3. Differentiating and integrating modes for C2 domain–mediated activation of cellular responses. (**A**) Surface plot showing the number of cells in the *z* axis. The maximal C2 domain translocation rate (*y* axis) was measured as the maximal increase in fluorescence intensity over a 2-s interval normalized to the maximal translocation amplitude after ionomycin addition. The integrated C2 domain membrane localization (*x* axis) was measured by integrating the fluorescence signal from the initial translocation until the time when C2 domains dissociated 85% away from the plasma membrane and was normalized by the product of the maximal ionomycin-induced translocation amplitude and the duration of the measurement (270 s). The four surface plots show the activity distributions for increasing agonist concentration: 0.01 nM (N = 510), 0.5 nM (N = 1496), 2 nM (N = 1673), and 100 nM (N = 2393). The surface plots were generated by 80 × 80 binning and 8 × 8 low-pass filtering. (**B**) Population-averaged rate and integrated translocation parameters measured at different PAF concentrations. The two overlaid graphs show the PAF concentration dependence of the averaged maximal translocation rate (blue downward triangles) and the averaged integrated activity (red upward triangles). Each data point in both of the graphs represents a separate experiment with 500 to 3000 cells.

parameters for downstream signaling. We determined whether the two observed C2 domain translocation patterns could selectively activate different signaling processes by comparing for each cell the integrated activity and the maximal rate of translocation. Figure 3A shows surface plots for different PAF concentrations of the number of cells (*z* axis) with a given maximal C2 domain translocation rate (*y* axis) and a given integrated plasma membrane localization (*x* axis). In addition to a basal state that is visible in the lower corner of the left and center panels in the top row of Fig. 3A, this analysis revealed two distinct signaling modes that appear as separated hills in the surface plot (Fig. 3A, top row, right): (i) a "differentiating" signaling mode with a maximal C2 domain translocation rate and a minimal integrated activity (Fig. 3A, top row, center and right), and (ii) an "integrating" signaling mode with the same translocation rate but with integrated activity increased by a factor of 10 to 30 (Fig. 3A, top row, right, and bottom left). Analysis of the population averages of these parameters shows that maximal translocation rates were triggered at low PAF concentrations, whereas significant integrated activities were triggered over a narrow range of higher PAF concentrations (Fig. 3B).

Our study introduces a broadly applicable technology (E-SCAT) for measuring the translocation of signaling proteins and domains in large numbers of individual cells. Thus far, we have measured significant increases in signal amplitude attributable to the receptor-triggered membrane translocation of cyan fluorescent protein (CFP)– and YFP-conjugated C2, PH, and C1 domains as well as of different PKC isoforms [Web fig. 2 (*10*)]. Using this technology, we found that the receptor-triggered translocation of C2 domains follows one of two discrete temporal patterns that depend on calcium release for transient membrane localization and calcium influx for persistent localization. Because Ca^{2+}-sensitive C2 domains are common regulatory motifs of diverse signaling proteins, each of these translocation responses can mediate a coordinated activation of different downstream targets inducing either a differentiating or an integrating signaling mode. This indicates that the selection between particular signaling responses can occur soon after receptor stimulation, before transcriptional activation. Our study suggests that measurements of translocation time courses in large cell numbers and the identification of discrete response patterns can be used as a general strategy to identify modes in dynamic signaling networks and to reduce network complexity.

References and Notes

1. P. Cluzel, M. Surette, S. Leibler, *Science* **287**, 1652 (2000).
2. J. E. Ferrell Jr., E. M. Machleder, *Science* **280**, 895 (1998).
3. M. A. Lemmon, K. M. Ferguson, *Biochem. J.* **350**, 1 (2000).
4. T. Pawson, *Nature* **373**, 573 (1995).
5. S. G. Rhee, *Annu. Rev. Biochem.* **70**, 281 (2001).
6. R. B. Sutton *et al.*, *Cell* **80**, 929 (1995).
7. J. Rizo, T. C. Südhof, *J. Biol. Chem.* **273**, 15879 (1998).
8. A. C. Newton, *Curr. Opin. Cell. Biol.* **9**, 161 (1997).
9. The PKCγ-C2 domain (*16*) was cloned into the YFP version of the pcDNA3 vector (Invitrogen). RBL cells stably transfected with the PAF receptor were obtained from R. Snyderman, Duke University (*25*). YFP fusion constructs were introduced into the RBL cells by microporation (*26*). PAF was obtained from Calbiochem (catalog number 510075).
10. For further details, see *Science* Online at www.sciencemag.org/cgi/content/full/295/5561/1910/DC1.
11. J. A. Steyer, W. Almers, *Nature Rev. Mol. Cell Biol.* **2**, 268 (2001).
12. F. Codazzi, M. N. Teruel, T. Meyer, *Curr. Biol.* **11**, 1089 (2001).
13. MATLAB (The Mathworks, Natick, MA) was used for the translocation analysis. An object recognition algorithm was developed to identify adherent cells as fluorescent spots. Attached cells had a basal fluorescence even when the fluorescent probe was cytosolic. The maximal area recorded per cell was 21 μm by 21 μm. Fluorescence intensity was monitored over time at each spot. Fluorescent spots that did not respond to ionomycin (final concentration 1 μM), that had saturated intensity, or that completely disappeared (dissociated) during the recording were eliminated from the analysis.
14. N. Verdaguer *et al.*, *EMBO J.* **18**, 6329 (1999).
15. A. Dessen *et al.*, *Cell* **97**, 349 (1999).
16. E. Oancea, T. Meyer, *Cell* **95**, 307 (1998).
17. Amino acid numbers are from full-length PKCγ (*16*).
18. S. Corbalan-Garcia, J. A. Rodriguez-Alfaro, J. C. Gomez-Fernandez, *Biochem. J.* **337**, 513 (1999).
19. M. J. Berridge, *Biochem J.* **312**, 1 (1995).
20. H. Gouy *et al.*, *Eur. J. Immunol.* **20**, 2269 (1990).
21. M. N. Teruel, unpublished data.
22. J. G. Hardman *et al.*, Eds., *Goodman & Gilman's The Pharmacological Basis for Therapeutics* (McGraw-Hill, New York, ed 9, 1996), pp. 38–39.
23. For such first-order signaling responses, the relevant signaling parameter is the product of a signal's amplitude and duration. For signals that change over time, such as the C2 domain translocation, the relevant signaling parameter for first-order processes is the integral of the amplitude of a signal over time.
24. The rate of increase of a signal becomes a key parameter if downstream signaling responses rapidly desensitize or inactivate. Desensitization and inactivation have been described in many signaling pathways and are best understood for channels and receptors (*27*, *28*).
25. H. Ali *et al.*, *J. Biol. Chem.* **269**, 24557 (1994).
26. M. N. Teruel, T. Meyer, *Biophys. J.* **73**, 1785 (1997).
27. M. V. Jones, G. L. Westbrook, *Trends. Neurosci.* **19**, 96 (1996).
28. E. Boue-Grabot, V. Archambault, P. Seguela, *J. Biol. Chem.* **275**, 10190 (2000).
29. A cylindrical lens was used to focus the laser onto a rotating holographic diffuser. The resulting line-shaped light source was then projected onto the edge of a glass plate that was ground to a 15° angle and polished with five increasingly finer steps to generate an optically plane surface (Labopol-2 grinder/polisher, Struers Inc., Westlake, OH).
30. Fluorescent images were taken with a Princeton Instruments 5-MHz Micromax charge-coupled device (CCD) camera at an excitation wavelength of 514 nm from a Melles-Griot 100-mW argon ion laser. The projection system was built from two camera objectives (Canon 50 mm, numerical aperture 0.35), with juxtaposed lenses, providing a 1:1 magnification (7 μm per pixel).

31. Supported by NIH grants HG00057 (M.N.T.) and CA83229 (T.M.) and by Alliance for Cell Signaling Bridging grant GM062144. We thank R. Tsien, L. Stryer, R. Aldrich, P. K. Jackson, and R. S. Lewis for stimulating discussions.

2 August 2001; accepted 25 January 2002